arXiv:1602.04013v1 [cond-mat.mes-hall] 12 Feb 2016

Method for determining the residual electron- and hole- densities about the neutrality point over the gate-controlled n ↔ p transition in graphene

Ramesh G. Mani[1]

[1]*Department of Physics and Astronomy, Georgia State University, Atlanta, GA 30303.*

(Dated: February 15, 2016)

The Hall effect, and the diagonal resistance, which indicates a residual resistivity $\rho_{xx} \approx h/4e^2$, are experimentally examined over the p↔n transition about the nominal neutrality point in chemical vapor deposition (CVD) grown graphene. A distribution of neutrality potentials is invoked in conjunction with multi-carrier conduction to model the experimental observations. From the modeling, we extract the effective residual electron- and hole- densities around the nominal neutrality point. The results indicate mixed transport due to co-existing electrons and holes in large area zero-band gap CVD graphene devices, which indicates domain confined ambipolar currents broadly over the gate-induced n ↔ p transition.

Graphene[1, 2] exhibits remarkable features such as massless Dirac fermions, an anomalous Berry's phase, and signatures of Hofstadter's spectrum,[3–6] while allowing for the gate-induced carrier type conversion, from holes to electrons, without crossing a bandgap.[7–10] When the Fermi level is placed at the Dirac point in monolayer graphene, one expects the *density* of carriers, n_q, i.e., electrons (n_e) and holes (n_h), to vanish, leading to a divergent Hall resistance, R_{xy}, and a diverging resistivity ρ_{xx}, since R_{xy} and ρ_{xx} are $\propto 1/n_q$. Remarkably, experiment has reported a finite, nearly quantized $\rho = \sigma^{-1} \approx h/4e^2$, reminiscent of the prediction $\sigma_{min} = e^2/h$ per massless Dirac channel,[7, 9] electron-hole puddles,[9, 11–13] along with Hall effect compensation.[1] Here, we examine vanishing- instead of diverging- Hall effect over the p↔n transition, in CVD graphene,[14] in addition to $R_{xy} \to 0$, as the diagonal resistance through the Dirac peak indicates $\rho_{xx} \approx h/4e^2$ at the nominal neutrality point. We reproduce these characteristics using a parabolic distribution $f(V_N)$ of neutrality potentials, V_N, in an ambipolar multi-conduction model.[16] The results serve to extract the effective residual electron- and hole- densities at the nominal neutrality point, and as a function of the gate voltage around the neutrality point. The observed simultaneous non-vanishing electron- and hole- densities in this zero bandgap material at liquid helium temperatures suggest that the applied current could be simultaneously carried by streams of electrons and holes within spatially separated current domains in these large area CVD graphene devices.

Monolayer graphene was prepared using the CVD technique,[14] processed into mm-scale devices, and measured in a low temperature magnet cryostat, see supplementary material.[15] The inset of Fig. 1(a) shows the graphene on SiO_2/Si, while figure 1(a) exhibits the Raman scattering spectrum. Here, the D-peak is small and the 2D-to-G intensity ratio, $I_{2D}/I_G = 2$, suggests monolayer graphene.[14] Figure 1(b) shows the diagonal resistance, R_{xx}, and R_{xy} vs. the magnetic field, B, at a back gate-voltage $V_G = 73$ V, close to the nominal neutrality voltage, $\nu = 72.8V$. This panel (Fig. 1(b)) shows a large ($\approx 8\%$) weak localization correction to R_{xx}.[8–10, 17–20] The $|R_{xy}| = 3.7$ ohms at $B = 0.5$ Tesla evaluates to $B/R_{xy}e = 8.5 \times 10^{13}$ cm^{-2} at a V_G where one expects $n_e < 1 \times 10^{12} cm^{-2}$.

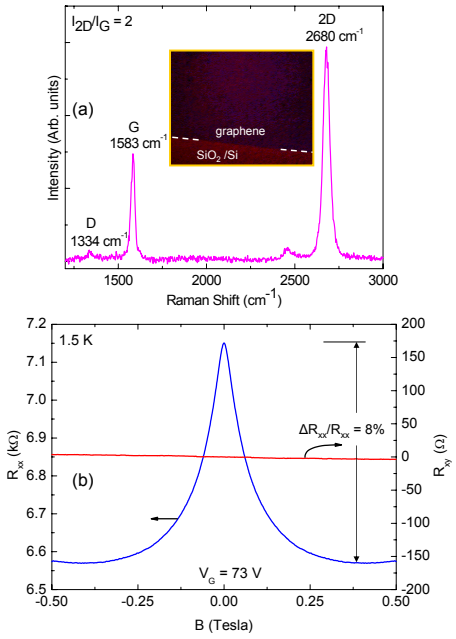

FIG. 1: (Color online) (a) The Raman intensity vs. the Raman shift for graphene-on-SiO_2/Si-substrate. The D-, G-, and 2D- peaks have been marked. The 2D-to-G intensity ratio, $I_{2D}/I_G = 2$, suggests monolayer graphene. (b) The diagonal resistance, R_{xx}, and the Hall resistance, R_{xy}, have been plotted vs. the magnetic field, B, for a gate-voltage $V_G = 73$ V. The figure indicates a relatively large (≈ 8 per-cent) weak localization correction.

The next figures provide an experimental overview of the approach to a vanishing Hall effect state at $V_G = \nu$. Figure 2(a) shows that R_{xx} changes non-monotonically with V_G, as R_{xx} initially increases, followed by a decrease

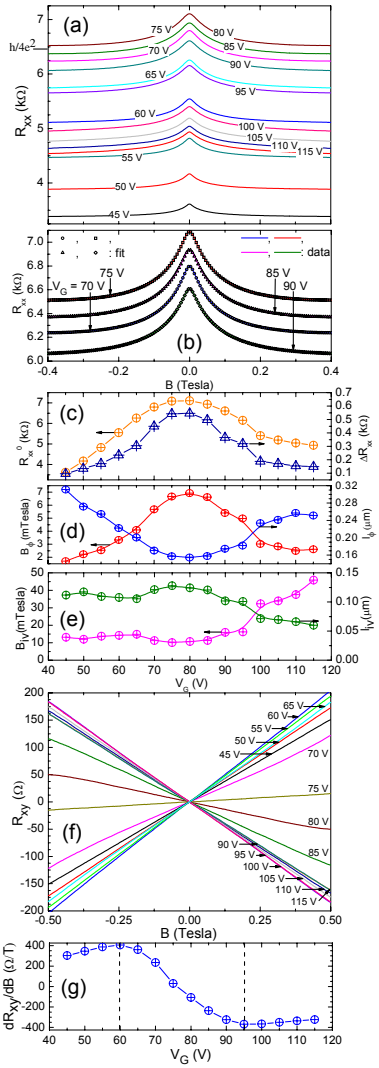

FIG. 2: (Color online) (a) At $T = 1.5$K, R_{xx} is plotted vs. B with V_G as parameter. Here, R_{xx} initially increases up to $V_G = 75$ V. For $V_G \geq 80$ V, R_{xx} decreases with increasing V_G. (b) Fits to graphene weak localization theory, see text. (c) The fit extracted zero-field resistance, R^0_{xx}, and the amplitude of the weak localization correction, ΔR_{xx}, are shown vs. V_G. (d) The fit extracted phase coherence field, B_ϕ and the phase coherence length l_ϕ are exhibited vs. V_G. (e) The fit extracted inter-valley field, B_{iv} and the inter-valley length l_{iv} are exhibited vs. V_G. (f) At $T = 1.5$K, the Hall resistance R_{xy} is plotted vs. B with V_G as a parameter. (g) Note the non-monotonic variation in dR_{xy}/dB vs. V_G.

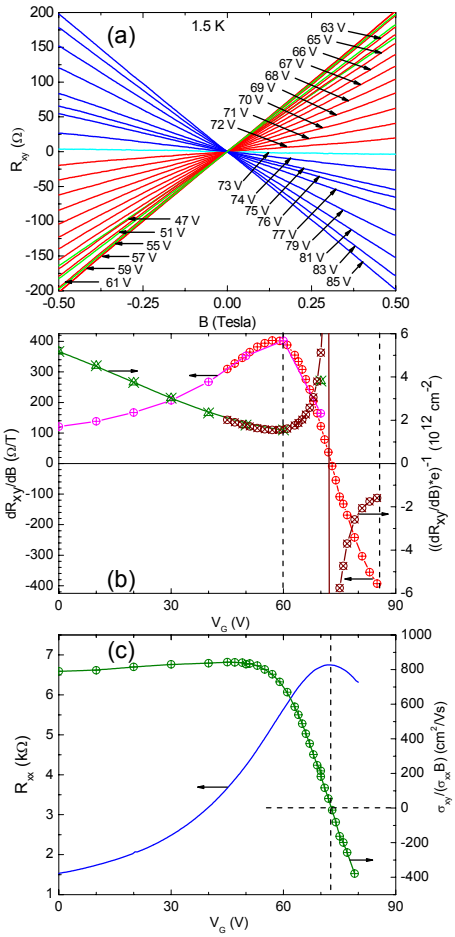

FIG. 3: (Color online) (a) The Hall resistance, R_{xy}, is exhibited vs. B for different V_G. The green (red) traces show a positive slope dR_{xy}/dB that increases (decreases) with V_G. The cyan trace marks the boundary between the red and dark blue traces. Dark blue traces show a negative slope. (b) dR_{xy}/dB evaluated from panel (a) are plotted as red symbols vs. V_G. The green and brown symbols show $1/((dR_{xy}/dB)e)$, the carrier density in a single carrier model. (c) R_{xx} (blue trace) peaks at the nominal neutrality point (dashed vertical line). The evaluated $\sigma_{xy}/(\sigma_{xx}B)$ (green symbols), would suggest a drop in the hole mobility over the range $55 \leq V_G \leq 72$V.

above $V_G = 80$ V. Here, $\nu \approx 77$ V. Also observable in Fig. 2(a) is the weak localization correction which increases towards $V_G = \nu$. Fig. 2(b) exhibits good data fits to weak localization theory,[19] see supplementary [15], on both the nominally hole- and nominally electron-side of $V_G = \nu$. Fig. 2(c) shows the fit extracted zero-field resistance, R^0_{xx}, and the weak localization amplitude, ΔR_{xx}, vs. V_G. At $V_G = 75V$, $R^0_{xx} = 7.1k\Omega$ and $R_{xx}(0.4T) = 6.5k\Omega$ lie within $\approx 10\%$ of $h/4e^2 = 6.45k\Omega$. Fig. 2(d) exhibits the fit extracted phase coherence field B_ϕ and the phase coherence length l_ϕ vs. V_G. The fit extracted inter-valley field, B_{iv} and the inter-valley length l_{iv} are exhibited vs. V_G in Fig. 2(e). In sum, the fits work equally well on either side of the nominal Dirac point, and the fit parameters, exhibited in Fig. 2(c)-2(e), suggest increasing "localization" with gate-induced carrier depletion.

Fig. 2(f) reports the Hall resistance. Here, the slope of R_{xy} vs. B is positive and increases with V_G up to $V_G = 60V$. From $60 \leq V_G \leq 75V$, the slope remains positive although now it decreases in magnitude with increas-

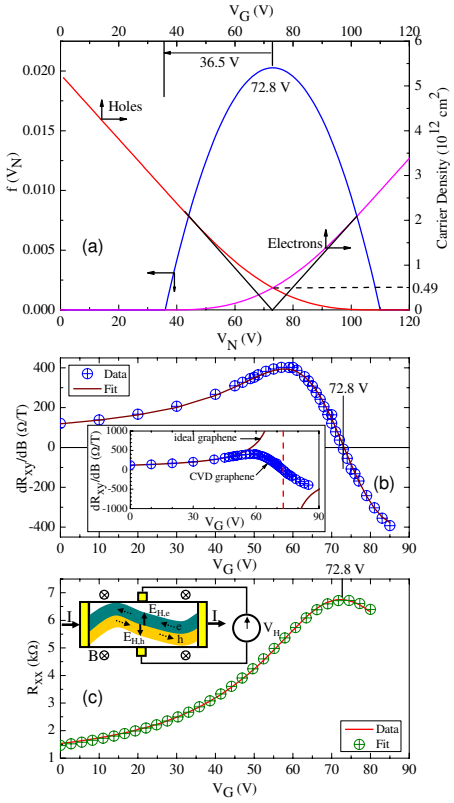

FIG. 4: (Color online) (a) The blue trace shows the distribution function, $f(V_N)$, of the neutrality voltages. The red and magenta traces show the effective hole and electron densities, respectively. The black lines show the hole and electron densities in ideal monolayer graphene. (b) The data (blue symbols) and best fit (brown curve) of the dR_{xy}/dB vs. V_G obtained for the effective carrier densities of panel (a). Inset: A comparison of the V_G dependence of dR_{xy}/dB in ideal monolayer graphene and CVD graphene. (c) The data (green symbols) and fit (red curve) of the R_{xx} vs. V_G obtained for the effective carrier densities of panel (a). Inset: Near the nominal neutrality point, coexisting electron and hole streams, with oppositely oriented Hall electric fields ($E_{H,e}$ and $E_{H,h}$), carry the applied current. The Hall effect then vanishes due to voltage compensation.

ing V_G. Above $V_G = 75V$, the slope turns negative and increases in magnitude up to $V_G = 100V$. Finally, the negative slope decreases in magnitude above $V_G = 100V$. Fig. 2(g) shows the non-monotonic variation in dR_{xy}/dB vs. V_G, where $dR_{xy}/dB = \Delta R_{xy}/\Delta B = R_{xy}(B)/B$ since $R_{xy}(0) = 0$. Here, the dashed lines mark an anomalous band where the $|dR_{xy}/dB|$ decreases in magnitude towards $V_G = \nu$ although n_q should decrease in this direction.

Characteristics over the crossover of the nominal neutrality point are examined at smaller V_G intervals in Fig. 3. In Fig. 3(a), for the green traces, the positive slope dR_{xy}/dB increases with V_G. For the red traces, the positive slope decreases with increasing V_G. The cyan trace, $V_G = 73V$ marks a boundary between the red and dark blue traces. [Data at this V_G appear in Fig. 1(b)]. For the dark blue traces, the slope is negative and it increases in magnitude with increasing V_G. dR_{xy}/dB evaluated from Fig. 3(a) are plotted as red symbols vs. V_G in Fig. 3(b). Magenta symbols represent other data not shown. Note that the dR_{xy}/dB increases with increasing V_G only up to $V_G \approx 60V$. Above $V_G = 60V$, the slope decreases with increasing V_G as it vanishes slightly below $V_G = 73$ V. For a further increase in V_G, dR_{xy}/dB becomes negative and increases in magnitude with V_G. Also shown with the green and brown symbols in Fig. 3(b), is $1/((dR_{xy}/dB)e)$, where $1/((dR_{xy}/dB)e)$ would equal the carrier density for single carrier conduction. Here, $1/((dR_{xy}/dB)e)$ decreases up to $V_G \approx 50$V as expected for hole depletion with increasing positive V_G via $n_h \approx C(\nu - V_G)$ where $C \approx 7.2 \times 10^{-10} cm^{-2}/V$. The trace then deviates from expectations as $1/((dR_{xy}/dB)e)$ increases with increasing V_G between $60 \leq V_G \leq 72$V, although one expects further hole depletion. Similarly, from slightly below $V_G = 73$V, increase in V_G should increase n_e, while the $1/((dR_{xy}/dB)e)$ (brown symbols) indicates opposite behavior.

The R_{xx} vs. V_G data at $B = 0$ are shown as the blue trace in Fig. 3(c). The peak $R_{xx} \approx 6.5k\Omega \approx h/4e^2$ at $V_G = \nu$. We evaluate $\sigma_{xy}/(\sigma_{xx}B)$, where σ_{xx} and σ_{xy} are the conductivity tensor components, and plot the result vs. V_G, see the green trace, in Fig. 3(c). This plot suggests that holes in this specimen exhibit an approximately constant mobility over the range $0 \leq V_G \leq 50V$. Then, above $V_G = 50V$, $\sigma_{xy}/(\sigma_{xx}B)$ decreases with increasing V_G as it vanishes at ν. At higher V_G, $\sigma_{xy}/(\sigma_{xx}B)$ changes sign indicating electron conduction as it increases in magnitude with V_G. Thus, a single carrier interpretation which associates $\sigma_{xy}/(\sigma_{xx}B)$ with μ would suggest, unphysically, that the mobility changes with V_G.

Since a single carrier interpretation leads to unphysically large n_q close to the Dirac neutrality point, where n_q ought to vanish, and setting $\sigma_{xy}/(\sigma_{xx}B) = \mu$ also leads to μ varying un-physically with V_G, see Fig. 3(c), we considered, in the first iteration, ambipolar conduction in a uniform-carrier-density, two carrier Drude model, where at each V_G, there occurs both an electron and a hole contribution at a constant density to the conductivities σ_{xx} and σ_{xy}, see supplementary.[15] Notably, this approach did not help to produce good fits of the data.

The large neutrality voltage, V_N, observed in CVD graphene on SiO_2/Si results from the combined gating effects of trapped charge in the SiO_2/Si substrate, charge donating impurities below the graphene,[21] and adsorbates on the graphene layer. It appeared plausible that such disorder effects could combine to produce a variation in the neutrality voltage across the mm-scale CVD graphene specimen. Thus, we introduced a distribution function, $f(V_N)$, for V_N with $\int f(V_N)dV_N =$

1, see supplementary.[15] Here, we focus upon the results obtained with the parabolic distribution, $f(V_N) = A(w^2 - (V_N - \nu)^2)$, blue curve of Fig. 4(a), which is non-vanishing only between $V_N = \nu \pm w$.

A distribution function $f(V_N)$ introduces a gradation in the neutrality voltage, and a non-uniformity in the carrier density across the specimen. Suppose, for the sake of discussion, that the spread in neutrality voltages occurs all in one direction, say, the x-direction, across the width (W) of a Hall bar device of length L, with the left edge of the Hall bar at $x = 0$ is at $V_N = \nu - w$ and the right edge of the Hall bar at $x = W$ is at $V_N = \nu + w$. Suppose the step size in V_N is ΔV_N, then the spread in V_N would correspond to a number of strips of constant V_N, which percolate from the bottom end of the Hall bar at $y = 0$ to the top end at $y = L$. (Scanning probe studies, see for example Fig. 3(a) of ref. [12], have suggested percolation of the hole and electron puddles over micron length scales). The spatial width, Δx_i, of these percolating strips at a particular V_N^i would be given by $\Delta x_i = W f(V_N^i)\Delta V_N$. The total conductance of the specimen system would equal the sum of the conductances of all these strips. For simplicity, assume that all the strips have the same mobility. Then, $\sigma_{xx} = (e\mu/(1 + (\mu B)^2)(1/W)(\sum n_i \Delta x_i)$. In neutrality voltage space, after separating out the electron and hole components, one obtains $\sigma_{xx} = (e\mu/(1 + (\mu B)^2)[C \int_{\nu-w}^{V_G}(V_G - V_N)f(V_N)dV_N + C \int_{V_G}^{\nu+w}(V_N - V_G)f(V_N)dV_N]$. Similarly, $\sigma_{xy} = (e\mu^2 B/(1+(\mu B)^2)[-C \int_{\nu-w}^{V_G}(V_G - V_N)f(V_N)dV_N + C \int_{V_G}^{\nu+w}(V_N - V_G)f(V_N)dV_N]$.

Using this model, we evaluated the diagonal resistance $R_{xx} = \rho_{xx}(L/W)$ and $dR_{xy}/dB = (R_{xy}(0.5T)/(0.5T))$. A least squares data-fit was carried out with ν and w as the fitting parameters. The blue trace in Fig. 4(a) illustrates the $f(V_N)$ that served to obtain the best data fit shown in Fig. 4(b) and Fig. 4(c). This $f(V_N)$ peaks at $\nu \approx 72.8V$ and exhibits a width $w = 36.5V$. The extracted effective electron and hole densities for the best fit $f(V_N)$ are also shown in Fig. 4(a). Here, the effective hole density at a particular gate voltage $V_G \leq \nu + w$ is $n_h^{eff.}(V_G) = C \int_{V_G}^{\nu+w}(V_N - V_G)f(V_N)dV_N$. Similarly, the effective electron density at $V_G \geq \nu - w$ is $n_e^{eff.}(V_G) = C \int_{\nu-w}^{V_G}(V_G - V_N)f(V_N)dV_N$. The notable features are that (a) for a broad range of V_G about $\nu = 72.8V$, one finds non-vanishing $n_e^{eff.}$ and $n_h^{eff.}$, unlike the expectations for n_e and n_h indicated by the black lines for ideal graphene, and (b) at $\nu = 72.8V$, the effective densities are given by $n_h^{eff.} = n_e^{eff.} = 0.49 \times 10^{12} cm^{-2}$. Thus, this approach helps us to determine the effective residual densities of electrons and holes at the nominal neutrality point. Fig. 4(b) shows the experimental dR_{xy}/dB data along with the best fit, while Fig. 4(c) shows R_{xx} data along with the best fit. These good fits suggest that the model captures the transport behavior observed in the measurements.

When the Fermi level in ideal monolayer graphene is brought towards the Dirac neutrality point, naively, one expects n_q to progressively vanish, leading to a divergent dR_{xy}/dB, see brown trace Fig. 4(b) (inset), with a discontinuity (dashed red line in Fig. 4(b), inset) in dR_{xy}/dB vs. V_G at the nominal neutrality point. Measurements for large area disordered CVD graphene devices shown here illustrate that the dR_{xy}/dB changes smoothly from positive to negative values over a broad range of V_G, and $dR_{xy}/dB = 0$ at $V_G = \nu$. Indeed, in experiment, one might set $V_G = \nu$ and obtain vanishing Hall effect, or close to it, as in Fig. 1, with stable and reproducible results.

This modelling suggests ambipolar transport over a wide range of V_G, about $V_G = \nu = 72.8V$, see Fig. 4(a), because there is a concurrent non-vanishing effective electron- and hole- density over a broad span of V_G. The model provided here is reminiscent of the uniform-carrier-density two carrier Drude model. However, this model differs on the point that instead of two carriers at fixed densities, there is a gradation in the density of both the electrons and the holes over the sample. If we set the effective hole density to the hole density, i.e., $n_h^{eff.} = n_h$, and the effective electron density to the electron density, i.e., $n_e^{eff.} = n_e$, then this model is formally similar to the two carrier Drude model. Thus, we can use the predictions of the two carrier ambipolar Drude model to understand some observations. For example, in the ambipolar two carrier model with $\mu_h = \mu_e = \mu$ and $\mu B << 1$, $dR_{xy}/dB = (1/e)(n_h - n_e)/(n_h + n_e)^2$. Thus, $dR_{xy}/dB \propto n_h - n_e$, and dR_{xy}/dB should vanish at $V_G = \nu$, where $n_h = n_e$, as observed in experiment, see Fig. 3(b) or Fig. 4(b). A qualitative picture, which suggests streams rather than puddles, for the $V_G = \nu$ condition is exhibited in Fig. 4(c), inset. At $V_G = \nu$, the applied current is equally split by symmetry between counter-propagating holes and electrons. In a magnetic field, the Hall electric field, E_H, within these hole- and electron- current domains will be oppositely directed, which will lead to a vanishing global Hall effect.[23, 24] Yet, the diagonal resistance/resistivity would remain finite due to the finite residual densities and the non-vanishing mobility. For the experimental parameters, this residual resistivity turns out to be $\approx h/4e^2$.[9] Here, the observed weak temperature dependence of the residual resistivity is attributed to weak localization and the relative temperature insensitivity of the transport parameters at the nominal neutrality point.[22] Fig. 4(c), inset, also helps to qualitatively understand small deviations from $V_G = \nu$: Deviation towards the hole regime, i.e, $V_G \leq \nu$, will increase the hole current at the expense of the electron current. Then, the hole Hall electric field will exceed the electron Hall electric field, yielding a net hole-like Hall effect. On the other hand, deviating towards the electron regime, i.e., $V_G \geq \nu$, will increase the electron

current at the expense of the hole current, yielding a net electron-like Hall effect.

[1] K. S. Novoselov, A. K. Geim, S. V. Morozov, D. Jiang, Y. Zhang, S. V. Dubonos, I. V. Grigorieva, and A. A. Firsov, *Science* **306**, 666-669 (2004).

[2] C. Berger, Z. M. Song, T. B. Li, X. B. Li, A. Y. Ogbazghi, R. Feng, Z. T. Dai, A. N. Marchenkov, E. H. Conrad, P. N. First, and W. A. de Heer, *J. Phys. Chem. B* **108**, 19912-19916 (2004).

[3] K. S. Novoselov, A. K. Geim, S. V. Morozov, D. Jiang, M. I. Katsnelson, I. V. Grigorieva, S. V. Dubonos, and A. A. Firsov, *Nature* **438**, 197-200 (2005).

[4] Y. Zhang, Y-W. Tan, H. L. Stormer, and P. Kim, *Nature* **438**, 201-204 (2005).

[5] L. A. Ponomarenko et al.,*Nature* **497**, 594-597 (2013).

[6] C. R. Dean et al., *Nature* **497**, 598-602 (2013).

[7] N. H. Shon and T. Ando, *J. Phys. Soc. Jpn.* **67**, 2421 -2429 (1998).

[8] C. Berger, Z. Song, X. Li, X. Wu, N. Brown, C. Naud, D. Mayou, T. Li, J. Hass, A. N. Marchenkov, E. H. Conrad, P. N. First, and W. A. de Heer, *Science* **312**, 1191-1196 (2006).

[9] A. K. Geim and K. Novoselov, *Nat. Mat'l.* **6**, 183-191 (2007).

[10] A. H. Castro-Neto, F. Guinea, N. M. R. Peres, K. S. Novoselov, and A. K. Geim, *Rev. Mod. Phys.* **81**, 109 - 162 (2009).

[11] E. H. Hwang, S. Adam, and S. Das Sarma, *Phys. Rev. Lett.*, **98**, 186806 (2007).

[12] J. Martin, N. Akerman, G. Ulbricht, T. Lohmann, J. H. Smet, K. von Klitzing, and A. Yacoby, *Nat. Phys.* **4**, 144-148 (2008).

[13] K. Nomura, and A. H. MacDonald, *Phys. Rev. Lett.* **98**, 076602 (2007).

[14] X. Li et al., *Science* **324**, 1312 - 1314 (2009).

[15] See supplementary material at http://dx.doi.org/10.1063/1.4940363 for a description of the material- and sample- preparation method, and other issues.

[16] R. G. Mani, A. Kriisa and W. Wegscheider, *Sci. Rep.* **3**, 2747 (2013) (doi:10.1038/srep02747).

[17] H. Suzuura and T. Ando, *Phys. Rev. Lett.* **89**, 266603 (2002).

[18] S. V. Morozov, K. S. Novoselov, M. I. Katsnelson, F. Schedin, L. A. Ponomarenko, D. Jiang, and A. K. Geim, *Phys. Rev. Lett.* **97**, 016801 (2006).

[19] E. McCann, K. Kechedzhi, V. Falko, H. Suzuura, T. Ando, and B. L. Altshuler, *Phys. Rev. Lett.* **97**, 146805 (2006).

[20] V. I. Falko, K. Kechedzhi, E. McCann, B. L. Altshuler, H. Suzuura, and T. Ando, *Sol. St. Comm.* **143**, 33-38 (2007).

[21] Y. Zhang, V. W. Brar, C. Girit, A. Zettl, and M. F. Crommie, *Nat. Phys.* **4**, 722-726 (2009).

[22] S. V. Morozov, K. S. Novoselov, M. I. Katsnelson, F. Schedin, D. C. Elias, J. A. Jaszczak, and A. K. Geim, *Phys. Rev. Lett.* **100**, 016602 (2008).

[23] A. V. Andreev, I. L. Aleiner, & A. J. Millis, *Phys. Rev. Lett.* **91**, 056803 (2003).

[24] R. G. Mani, J. H. Smet, K. von Klitzing, V. Narayanamurti, W. B. Johnson, and V. Umansky, *Nature* **420**, 646-650 (2002).